

A phenotypic switch in the dispersal strategy of breast cancer cells selected for metastatic colonization

Article

Accepted Version

Butler, George, Keeton, Shirley J., Johnson, Louise J. ORCID logoORCID: <https://orcid.org/0000-0002-0006-1511> and Dash, Philip R. (2020) A phenotypic switch in the dispersal strategy of breast cancer cells selected for metastatic colonization. *Proceedings of the Royal Society B: Biological Sciences*, 287 (1940). ISSN 0962-8452 doi: <https://doi.org/10.1098/rspb.2020.2523> Available at <https://centaur.reading.ac.uk/94720/>

It is advisable to refer to the publisher's version if you intend to cite from the work. See [Guidance on citing](#).

Published version at: <https://doi.org/10.1098/rspb.2020.2523>

To link to this article DOI: <http://dx.doi.org/10.1098/rspb.2020.2523>

Publisher: Royal Society Publishing

All outputs in CentAUR are protected by Intellectual Property Rights law, including copyright law. Copyright and IPR is retained by the creators or other copyright holders. Terms and conditions for use of this material are defined in the [End User Agreement](#).

www.reading.ac.uk/centaur

CentAUR

Central Archive at the University of Reading

Reading's research outputs online

Title

A phenotypic switch in the dispersal strategy of breast cancer cells selected for metastatic colonisation

Authors

George Butler,¹ Shirley Keeton,¹ Louise Johnson¹, Philip Dash^{1*}

Affiliations

¹ School of Biological Sciences, University of Reading, UK

*Corresponding author

Email: p.r.dash@reading.ac.uk

1 **Abstract**

2 An important question in cancer evolution concerns which traits make a cell likely to successfully
3 metastasise. Cell motility phenotypes, mediated by cell shape change, are strong candidates. We
4 experimentally evolved breast cancer cells *in vitro* for metastatic capability, using selective regimes
5 designed to simulate stages of metastasis, then quantified their motility behaviours using computer
6 vision. All evolved lines showed changes to motility phenotypes, and we have identified a previously
7 unknown density-dependent motility phenotype only seen in cells selected for colonisation of
8 decellularized lung tissue. These cells increase their rate of morphological change with an increase in
9 migration speed when local cell density is high. However, when the local cell density is low, we find the
10 opposite relationship: the rate of morphological change decreases with an increase in migration speed.
11 Neither the ancestral population, nor cells selected for their ability to escape or invade extracellular
12 matrix-like environments, display this dynamic behavioural switch. Our results suggest that cells
13 capable of distant site colonisation may be characterised by dynamic morphological phenotypes and
14 the capacity to respond to the local social environment.

15

16

17

18

19

20

21

22

23

24

25

26

27

28

29

30

31

32

33

34 **Main Text**

35

36 **Introduction**

37

38 Metastasis is a form of long-range dispersal (1,2) and central to understanding how cancers
39 metastasise is understanding how cells migrate (3,4). During migration, as cancer cells become
40 more invasive and begin to migrate independently, they adopt an altered morphology, typically
41 taking on elongated shapes characteristic of epithelial-mesenchymal transition (EMT) (5,6). This
42 change in cellular morphology is an important marker of migratory state (7,8). Quantitative
43 measures of cell morphology taken from static images have been shown to effectively
44 differentiate between cancer cell lines with high and low metastatic potential (9,10). However,
45 there are important aspects of migratory behaviour linked to metastasis that cannot be measured
46 from static images.

47 Successful metastasis requires a cell to navigate through a series of sequential steps known as
48 the metastatic cascade. The cascade begins with a cell escaping from the primary tumour before
49 migrating through the extracellular matrix (ECM) towards a nearby blood vessel. The cell must
50 then intravasate into the blood before it is carried around the body. After reaching a distant site
51 the cell then needs to extravasate from the blood and invade the foreign tissue. Finally, the cell
52 must reinitiate aggressive proliferation enabling a secondary tumour to form (11).

53 In addition to the cellular changes needed for metastatic success, environmental changes are
54 also necessary for a cell to metastasise (12). This is evident at the onset of cellular dispersal
55 where nearby collagen fibres are straightened perpendicular to the tumour boundary (13). The
56 straightened fibres then act as a pathway for future migrants in turn improving their migratory
57 success (14). This dynamic cell-environment interplay continues throughout the metastatic
58 cascade.

59 To identify the precise changes in cell phenotype that are associated with metastatic success, it is
60 preferable to compare cell lines that differ only in their ability to metastasise. Experimental
61 evolution (15), a powerful approach that has led to major advances in evolutionary biology, is now
62 being applied to cancer evolution and provides the means to generate such cell lines (16,17).
63 Initially identical populations of cancer cells can be selected in replicate for specific capabilities
64 (18). We experimentally evolved populations of cancer cells using selective regimes
65 corresponding to three separate stages of metastasis (19,20): escape from the primary tumour,
66 invasion of foreign tissue, and distant site colonisation.

67 Distant site colonisation, the rate-limiting step of metastasis (21), requires a cell to migrate
68 through the unpredictable microenvironment of the primary tumour (22) and into the novel
69 environment of the distant metastatic site (11). Success in both stages is achieved, in part, by the
70 cell's capacity to detect and respond to changes in the environment (23-26). Cells selected for
71 distant site colonisation might therefore be expected to be more reactive to environmental
72 changes, and as such display a greater degree of morphological change in response. We would
73 also expect morphological change to be positively correlated with migration speed in successfully
74 metastasizing cells, because a faster-moving cell will experience a greater degree of
75 environmental variation over a given time period, and therefore change its morphology more
76 rapidly in response.

77 To test these hypotheses, we have combined an experimental evolution framework with video
78 microscopy and novel statistical analysis that quantifies morphological change in individual cells
79 over time. This approach has identified unique cell behavioural phenotypes that may be
80 advantageous for successful metastasis.

81 **Materials and Methods**

82 Evolved population summary

83 We used experimental evolution methods (15) on an initial population of MDA-MB-231 breast
84 cancer cells (Figure. 1), subjecting them to three separate selective regimes. The experimental
85 selective regimes were designed to be similar to those experienced whilst traversing the
86 metastatic cascade (11). We also froze two biological replicate *ancestor* populations (Figure. 1) at
87 the start of the experiment to act as a control for comparison with our evolved lines.

88 We selected escape populations (Figure. 1) by tightly packing cells into a high density core of
89 collagen and then allowing them to escape outwards into a low density collagen outer ring (27).
90 After 10-14 days the cells that had escaped into the outer collagen ring were recovered from the
91 matrix, expanded and then seeded back into a new collagen escape assay, completing one round
92 of selection. In total, 7 rounds of selection were applied to each of four biological replicate escape
93 populations. The high density collagen core and the low density outer collagen ring were both
94 three-dimensional (3D) culture environments designed to be similar to those experienced during
95 tumour dissemination.

96 We selected *invasion* populations (Figure. 1) following a similar protocol to the escape
97 populations whereby repeated consecutive rounds of selection were applied. In contrast to the
98 escape assay, however, cells moved from a 2D to 3D environment, similar to the change in
99 environment experienced during the arrest of a cell at a distant site. The cells were seeded
100 around the outside of a Matrigel island - a synthetic basement membrane matrix widely used in
101 cell culture - and left to invade. After 7 days the cells were collected from the Matrigel, expanded
102 and seeded around the outside of another Matrigel island. This process was repeated 15 times
103 for each of the four biological replicate populations over the course of the 6 month experiment.

104 We selected *colonisation* populations (Figure. 1) by culturing cells on a piece of decellularized rat
105 lung, which acted as a scaffold for growth similar to that experienced by cells colonizing a distant
106 site (27). The protocol involved cells being seeded onto a decellularized scaffold and left to
107 colonize over a 6 month period. Decellularized tissue is generated by removing all cells from a
108 piece of tissue such that only the extracellular matrix is left. At the end of the experiment cells
109 were released from the scaffold, ensuring that the population represented cells from within the
110 tissue core as well as the edges. Again, this selection was applied to-four biological replicate
111 populations.

112 Finally, all twelve experimentally evolved cell populations were frozen and then thawed alongside
113 the ancestor populations prior to experimental analysis. This step ensured that any selective
114 pressure from the freezing-thawing process was constant across all treatments and replicate
115 populations.

116 Experimental assays

117 Escape Assay

118 Initially, MDA-MB-231 cells (LGC) were encapsulated in a 2mg/ml collagen gel (rat-tail collagen
119 type 1, First Link) and set into a 24-well plate which was used as a mould (750,000 cells per gel,
120 Greiner Bio-One). The collagen gels were compressed for 2 minutes as described in (27), then
121 set into a 1mg/ml low density collagen gel (rat tail collagen type 1, First Link). Once set, cell
122 culture medium (Dulbecco's Modified Eagles Medium (DMEM) supplemented with 10% Fetal
123 Bovine Serum (FBS), and Penicillin 100 µg/ml, Streptomycin 100 U/ml (Gibco, Fisher Scientific))
124 was added over the top. Medium was replaced every 3-4 days. After 10-14 days, the
125 compressed collagen disc was separated from the low density collagen and collagenase type 1
126 diluted in phospho-buffered saline solution (Gibco, Fisher Scientific) used to retrieve the cells
127 from the collagen matrix, 200 U/ml for compressed collagen and 100 U/ml for low density
128 collagen. Cells in collagenase/PBS were incubated at 37°C in a stirred water-bath at 45 rpm for
129 30-60 minutes, then washed in Phospo-buffered saline solution (PBS, Gibco Fisher Scientific).

130 Cells extracted from the compressed collagen were placed in liquid nitrogen storage and those
131 collected from the low density collagen were seeded into 2mg/ml collagen gel with medium over
132 for population expansion. Once expanded, cells were retrieved from collagen using collagenase
133 in PBS then seeded into 2mg/ml collagen for compression or frozen at -80°C and transferred to
134 liquid nitrogen for storage.

135 Invasion Assay

136 MDA-MB-231 cells (LGC) were re-suspended in PBS, and seeded around the outside of a
137 5mg/ml set Matrigel island in a 6-well plate Matrigel (#35623, Corning), was diluted using DMEM
138 without supplements. Cells were seeded in excess at the island margins, with around 40,000 cells
139 seeded in 200 μ l per experiment for the initial set-up. Cells were left to settle and adhere to the 2D
140 surface for 60 minutes then cell culture medium added over the top (DMEM supplemented with
141 10% FBS, and penicillin 100 μ g/ml, streptomycin 100 U/ml). Medium was changed every 3-4
142 days and cells were harvested after 7 days. Cells were retrieved from Matrigel using Cell
143 Recovery solution (#354253, Corning) on ice for 45-60 minutes, washed with ice cold PBS then
144 reseeded into Matrigel at 5mg/ml to expand cell numbers. After 7 days the cells were released
145 from Matrigel using cell recovery solution as described above (typically 400,000 – 500,000 per
146 gel), re-suspended in PBS and seeded in excess around the outside of a new Matrigel island
147 (5mg/ml) for the next round of the 2D/3D invasion assay or cells were frozen at -80°C and
148 transferred to liquid nitrogen for storage.

149 Colonisation Assay

150 Rat lung was retrieved from 9 week old Wistar rats (Envigo) and flash frozen. It was then thawed
151 and decellularized using repeated rounds of treatment following an adapted version of the
152 protocol published in (28). Briefly: frozen lung was thawed and cut into small pieces of around
153 100mg, which were then placed into deionized water (ddH₂O), stirred at 60 rpm for 16 hours at
154 4°C. Lung tissue was treated with 0.02% trypsin/0.05% EDTA for 60 minutes at 37°C at 60 rpm,
155 3% Triton-X 100/PBS for 70 minutes, 1M sucrose/PBS for 30 minutes, 4% deoxycholate/ddH₂O
156 for 60 minutes, 0.1% peracetic acid in 4% ethanol for 120 minutes, PBS for 5 minutes, and finally
157 twice in ddH₂O for 15 minutes. The tissue was washed thoroughly between each treatment with
158 ddH₂O. De-cellularization was checked between rounds using epifluorescence microscopy and
159 staining with DAPI H1200 Vectashield (Vectorlabs) to identify whether cell nuclei remained within
160 the matrix structure. Decellularized lung tissue was freeze-dried and stored in an airtight
161 container.

162 Using decellularized lung as a culture matrix: tissue was soaked in 70% ethanol, washed with
163 PBS and then rehydrated in PBS pH 7.2 (Gibco) in a tissue culture incubator for 5 days, then
164 soaked in cell culture medium (DMEM supplemented with 10% FBS and penicillin/streptomycin
165 as described above) for 48 hours. Cells grown in 2D tissue culture flasks were trypsinized, re-
166 suspended in medium then 750,000 cells added in low volume of medium (100-150 μ l) over the
167 decellularized lung tissue in a 6-well plate and left to adhere for 2 hours. Medium was then
168 added over the top so that the decellularized lung rafts floated. Rafts were transferred to new
169 wells when the bottom of the well was confluent with shed and adhered cells. To feed the cells
170 growing in/on the raft, ½ of the medium (2ml of 4ml) was aspirated and replaced every 2-4 days.
171 After 140 and 189 days, rafts were retrieved from medium, washed with PBS and cells harvested
172 by incubating in: collagenase I (170 U/ml, Gibco 17018-029), collagenase IV (170 U/ml, Gibco
173 17104-019), elastase (0.075 U/ml, Sigma E7885) (based on the protocol described in (29))
174 incubated at 37°C 45rpm in a stirred water-bath, then washed twice with PBS before seeding in
175 2D tissue culture plates for expansion. Expanded cells were then frozen at -80°C and transferred
176 to liquid nitrogen for storage.

177 Time-lapse microscopy

178 Cells were retrieved from liquid nitrogen, cultured in 2D tissue culture flasks (25cm² or 75cm²
179 Greiner bio-one), trypsinized and seeded into 6-well plates (Greiner bio-one) at 10-15% cell
180 confluence. Time-lapse movies were made for 12 hour periods with images taken at 2 minute
181 intervals, using a Nikon TiE phase contrast microscope with an environmental chamber (37°C)
182 and moveable platform stage. x10 Plan Apo DIC L Lens was used in conjunction with an
183 intermediate magnification changer set to x1.5 to give x15 magnification. NIS Elements software
184 was used for image capture.

185 Cell Tracking

186 All cells that were present in each time-lapse video were tracked using the Usiigaci pipeline (30).
187 The neural network was trained on 300 randomly selected images that were manually annotated
188 using ImageJ (31). The manually annotated images were than randomly split so that 80% were
189 used for training and a further 20% were used for testing, 240 images in the training set and 60 in
190 the test set. The 240 training images were then further split for training and validation 90:10 so
191 that 216 images were used for training and 24 for validation. We trained 3 neural networks using
192 the same 240 images however different images were used for the training and validation stage
193 each time. All hyperparameter settings were the same as Usiigaci protocol except the gradient
194 clip norm was increased to 10. We trained the network on all layers over 300 epochs with the
195 learning rate starting at 0.01 and decreasing by an order of magnitude every 100 epochs.

196 Once the morphologies had been segmented we tracked them through time using the inbuilt
197 semi-automated Usiigaci tracker. After tracking we manually checked the segmented
198 morphologies and corrected any errors. We checked for cases whereby a cell had divided, been
199 mis-identified or incorrectly segmented. Finally we excluded the 30 minutes prior to and after a
200 cell division to remove the rounded morphologies typical of cell division from our analysis.

201 Quantifying values

202 All values were quantified using a custom-built pipeline in Python (32) that can be found on
203 GitHub, https://github.com/george-butler/2d_microscopy, any reference to distance refers to the
204 Euclidean distance. The morphology was quantified using the first 20 Zernike moments. Zernike
205 moments capture the information that is encoded in a shape and translate it into a high
206 dimensional vector, in a similar fashion to spatial location being represented by Cartesian
207 coordinates. When taken to a high enough degree, Zernike moments are capable of representing
208 every shape uniquely and are invariant to rotation, scale and translation (33). We followed the
209 methods of (10) to pre-process the morphologies and make them invariant to scale and
210 translation. We determined that 20 Zernike moments were adequate to quantify the morphology
211 of each cell by plotting the mean squared error against the number of moments (34) and finding
212 where the gradient approached 0.

213 Statistical analysis

214 All statistical analysis was performed in R (35) and Figures 3-5 were made using GGPlot (36). All
215 code and corresponding data can be found on GitHub, <https://github.com/george->
216 [butler/2d_microscopy/tree/master/statistical_analysis](https://github.com/george-butler/2d_microscopy/tree/master/statistical_analysis). A cell needed to appear in at least 30
217 frames to be included in our analysis and be present for at least 75% of the track. Some cells
218 were not detected in a given frame or had to be removed due to being incorrectly segmented.
219 Throughout our analysis we used linear mixed models to account for the differences between
220 replicate populations within the four treatments (37). The mean rate of morphological change and
221 the mean speed of migration were calculated through the use of an intercept only linear mixed
222 population with independent intercepts for each treatment. The rate of morphological change
223 model is defined below:

224 Rate of morphological change = $\alpha + \beta_1$ (speed of migration) + β_2 (distance to nearest
225 neighbour) + β_3 (speed of migration) * (distance to nearest neighbour) + (1|well id)

226

227 The model was selected through forward selection whereby parameters were only included if they
228 were significant at the 5% level. The marginal R² values were calculated using the method
229 detailed by (38).

230

231 **Results**

232

233

234 Quantifying dispersal in evolved populations

235 To analyse their dispersal behaviour cells were placed onto 2D tissue-culture plates and their
236 migration was recorded over a 12-hour period , with images taken at two-minute intervals. The 2D
237 plastic environment was intentionally chosen as a neutral testing environment and to ensure that
238 the morphology could be clearly seen without the use of fluorescent tags, a factor that might have
239 applied an additional selective pressure (39). The cells were tracked through the use of a semi-
240 automated pipeline, Usiigaci (30), that combined a convolutional neural network with our own
241 manually annotated images to trace the morphology of each cell at every time point (Figure. 2A).

242 We extracted three quantitative measures per cell per frame of time-lapse video: morphology,
243 speed and the distance to the closest neighbouring cell. Morphology was quantified using Zernike
244 moments. Zernike moments (33) have been used previously to quantify cancer cell morphology in
245 fixed populations (10) and are a method that captures all of the morphological information
246 available rather than needing to make a prior decision about which morphological features might
247 be important i.e. the length of a cell. The rate of morphological change is then measured as the
248 distance between the vector of moments in frame t and $t+1$ relative to the time between frames
249 (Figure. 2B). Speed of migration was calculated from the change in spatial location between
250 consecutive frames (Figure. 2C). The distance to the closest neighbour cell was calculated as the
251 shortest distance from the edge of the cell contour to another neighbouring cell contour without
252 crossing the body of the cell (Figure. 2D). Finally the average was calculated for each metric over
253 the entire trajectory of the cell, providing a summary of the dispersal phenotype of each cell.

254 After extracting these three metrics we sought to evaluate whether the rate of morphological
255 change or the speed of migration was significantly different among the four treatments. We used
256 an analysis of variance (ANOVA) to compare the mean rate of morphological change and the
257 mean speed of migration across all populations; differences in wells were accounted for as a
258 random effect. We found that there was significant variation among population in their mean rate
259 of morphological change ($p = 0.0296$, $N = 813$). We then conducted a post-hoc Bonferroni
260 multiple comparison test to identify which populations were different, controlling for any possible
261 between-replicate variation through the use of a random effect. Escape populations had a
262 significantly higher rate of morphological change compared with the invasion populations, ($p =$
263 0.0152 , $N = 813$; Figure. 3). There was no significant difference in the mean speed of migration
264 among the four treatments.

265

266 Speed of migration predicts rate of cell-morphological change in evolved populations

267 Next we investigated how the morphological behaviour of a cell related to its speed and its social
268 environment. We fitted a linear mixed model across our data whereby the rate of morphological
269 change is dependent on the speed of migration, the distance to the nearest neighbouring cell and
270 the interaction of the two, as detailed in our Methods. We set treatment as a fixed effect and

271 allowed intercepts and slopes to vary between treatments. The significant parameters were then
272 used to fit a reduced model to the ancestor, escape and invasion populations (Figure. 4).

273 In the ancestor populations neither the speed of migration nor the distance to neighbouring cells
274 significantly affected the rate of morphological change. We proceeded by fitting an intercept only
275 model to our data (Figure. 4). However, the intercept model explained only a small proportion of
276 the variance, (marginal $R^2 = 0$). This might suggest that the rate of morphological change is highly
277 stochastic, or that it depends on factors not included in our model.

278 In contrast, in both escape and invasion populations, the rate of morphological change is
279 significantly positively correlated with the speed of migration, ($\beta = 0.680$ and 0.319 respectively:
280 Figure. 4). Furthermore, the escape and invasion models both explain a significant proportion of
281 the variation (marginal $R^2 = 0.347$ and 0.099 respectively). To ensure that our results were not
282 affected by a small cluster of potential outliers we repeated the same analysis after having
283 removed influential data points, defined by a Cook's distance $> (4 / N)$ where N is the sample
284 size (40).

285 The slope of the relationship is steeper for escape than for invasion populations suggesting that
286 selection for escape may favour cells that can change their morphology rapidly when migrating at
287 a high speed. This might be a result of the collagen escape assay being a 3D to 3D environment
288 compared with the 2D to 3D environment of the Matrigel invasion assay. However, this also could
289 be due to the different number of rounds of selection between the two assays, or difference in the
290 strength of selection within each.

291

292 Spatial density affects morphological dynamics

293 The colonisation populations displayed a complex morphological behaviour dependent on the
294 speed of migration, the distance to the nearest neighbouring cell and the interaction of the two: as
295 the distance between neighbouring cells increases, the relationship between the rate of
296 morphological change and the speed of migration becomes negative (Figure. 5A). When close to
297 a neighbouring cell, the rate of morphological change is positively correlated with the speed of
298 migration: a faster speed of migration results in a higher rate of morphological change. However,
299 when the distance between neighbouring cells is large and a cell is isolated, the rate of
300 morphological change is negatively correlated with the speed of migration: a faster speed of
301 migration has a lower rate of morphological change. We repeated the same analysis after the
302 removal of any influential data points and found that the interaction term was still significant in
303 these colonisation populations (Fig. S1). We also found that the colonisation model explained a
304 significant proportion of the variation in the rate of morphological change (marginal $R^2 = 0.236$).

305 Next we sought to determine whether the switch in morphological behaviour with distance was
306 gradual or sudden. To investigate this hypothesis, we centred the nearest neighbour data at a
307 distance x and then refitted the same morphological change model. After fitting the model, we
308 evaluated whether the speed of migration was significant in the model. If the speed of migration is
309 not significant then we know that at a distance x there is not a significant difference in the rate of
310 morphological change for cells migrating at different speeds. We can then repeat the same
311 method for different values of x to find a range of distances over which the speed of migration is
312 not significant. The smaller the range the more sudden the switch.

313

314 We found that for nearest neighbour distances between $57.9\mu\text{m}$ and $147.2\mu\text{m}$ the speed of
315 migration is not significant in our model, as seen by the shaded region in Figure. 5B. Therefore, at
316 distances $< 57.9\mu\text{m}$ or $> 147.2\mu\text{m}$ the speed of migration is significantly related to the rate of
317 morphological change. The small range of distance values suggests that the cells have a high
318 degree of sensitivity to the location of neighbouring cells. Interestingly, the range of distance
319 values coincides with values from the literature whereby cells within a tumour core have been

320 seen to display a correlated mode of migration at spatial distances < 50µm compared with
321 distances greater than 250µm (41).

322

323 Discussion

324

325 We have conducted novel phenotypic analysis across experimentally evolved populations of
326 MDA-MB-231 breast cancer cells to investigate their behaviour during dispersal. Combining
327 experimental evolution with computer vision we have generated a multidimensional data set that
328 quantifies single cell dispersal dynamics within each population. In turn we have built a
329 continuous data driven morphological model that has uncovered fundamental dispersal behaviour
330 at a cellular level and is capable of distinguishing cells selected for colonisation.

331 The flow of migratory cells through the microenvironment creates a landscape that is
332 heterogeneous both spatially and temporally (42). This landscape variability might in turn explain
333 the correlation between the rate of morphological change and the speed of migration for both the
334 escape and invasion populations (Figure 4). The collagen escape and Matrigel invasion assays
335 used to select the escape and invasion populations are porous and complex (43) but yet they are
336 also malleable. The malleability of these two environments means that large structural changes
337 can occur and thus migration routes that were previously accessible may become blocked.
338 Therefore, a cell may need to respond to its environment by changing its morphology to ensure
339 that it can continue to migrate and does not become trapped. Likewise, as the speed of migration
340 increases, an increase in the rate of morphological change might be necessary to ensure that the
341 cells aren't temporarily stuck by any potential obstacles. This would also explain why there is no
342 correlation in the ancestor populations where the environment remains constant and there would
343 therefore be no selective advantage to this behaviour.

344 Distant-site colonisation requires a cell to switch from a mode of long-range dispersal and focus
345 on re-initiating aggressive proliferation; the subsequent increase in local cell density may reduce
346 available space and thus intensify competition. A similar selective pressure can be seen in our
347 experimental assays. In contrast to the ancestor, escape and invasion populations, where cells
348 are periodically moved to a new expansive environment, the colonisation population remain fixed.
349 As such in addition to the structural changes that occurred in the microenvironment there was a
350 high density of cells migrating locally so cells themselves could block potential migration routes,
351 and therefore might explain the significance of the neighbour location in our model. This
352 hypothesis would also explain the interaction that is observed between neighbouring cells. If a
353 cell is migrating at a high speed and is close to other neighbouring cells, then changing its
354 morphology rapidly might be necessary to avoid other cells that are changing location
355 dynamically. However, when isolated the location of neighbouring cells is no longer of concern
356 and thus a reduction in the rate of morphological change might allow a cell to conserve
357 resources.

358 The significance of the neighbour sensitivity may also suggest that the ability of a cell to sense
359 contact has been re-acquired within the colonisation population. A loss of contact inhibition is
360 seen as one of the earliest developments in cancer progression as it allows aggressive
361 proliferation to ensue, which in turn gives rise to the formation of a primary tumour (44). However,
362 the high degree of neighbour sensitivity seen in Figure. 5 questions whether contact sensing is in
363 fact lost, or instead down-regulated earlier in the metastatic cascade. If true, this could suggest
364 that cells selected for distant-site colonisation are able to vary their own contact sensing ability
365 dependent on the exogenous environmental stresses they encounter.

366

367 In summary, we have shown that evaluating cell morphology as a dynamic process provides
368 novel insight into the behaviour of breast cancer cells, and furthers our understanding of the
369 phenotypic route to metastasis. A pivotal next step will be evaluating morphological dynamics
370 within a native 3D environment (45) and in the vicinity of stromal cells such as a fibroblasts which

371 are known to have a critical role in metastasis (46). The presence of stromal cells might also
372 change the relationship seen within our escape and invasion populations, as cells would then be
373 able to interact via matrix metalloproteinases. Thus, rather than needing to change their
374 morphology quickly to prevent being trapped, they could exploit the matrix metalloproteinases to
375 cut them free, as seen previously during metastatic dispersal (47). It would also be of value to
376 subject multiple starting cell lines to a similar selective regimes, in case the MDA-MB-231 line
377 used here behaves atypically. However, we believe that this work highlights the power of
378 phenotypic analysis in discovering the complex emergent behaviours that would not have been
379 apparent from genetic data .

380 **Acknowledgments**

381
382 We thank Chris Venditti and Mark Pagel for critical reading of the manuscript.
383

384 **Author Contributions**

385 G.B, S.K, L.J and P.D conceived and designed the study. S.K evolved the populations and
386 collected the time-lapse data. G.B developed the methodology and performed the formal
387 analysis. L.J and P.D supervised the work. G.B wrote the manuscript. All authors gave final
388 approval for publication and agree to be held accountable for the work performed therein.

389

390

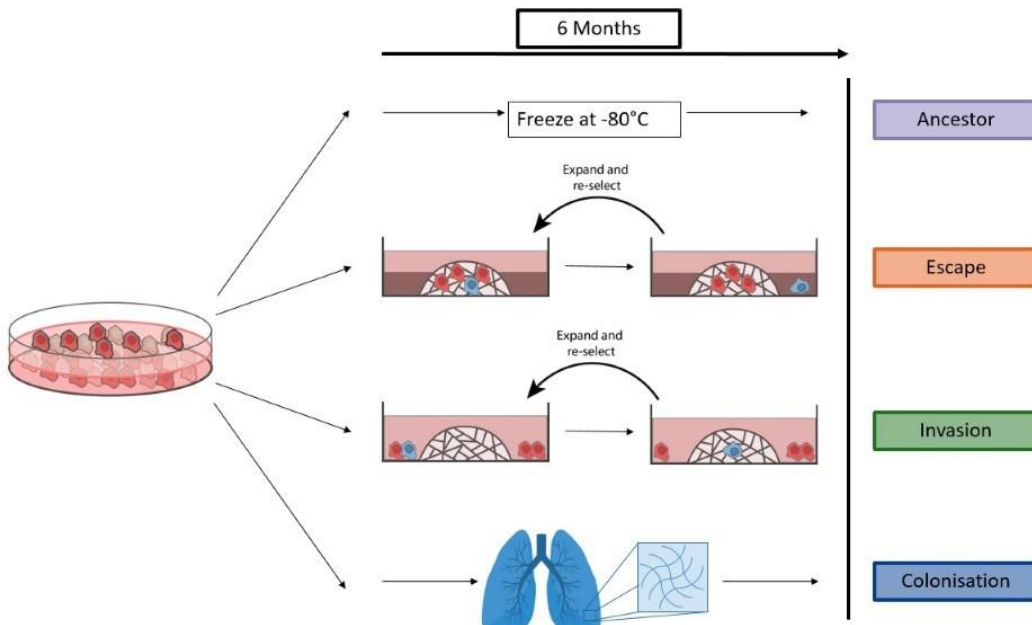
391 **References**

- 393 1. Amend SR, Roy S, Brown JS, Pienta KJ. Ecological paradigms to understand the dynamics of
394 metastasis. *Cancer Lett.* 2016;237–42.
- 395 2. Tissot T, Massol F, Ujvari B, Alix-Panabieres C, Loeuille N, Thomas F. Metastasis and the
396 evolution of dispersal. *Proc R Soc B Biol Sci.* 2019;20192186.
- 397 3. Paul CD, Hung W-C, Wirtz D, Konstantopoulos K. Engineered Models of Confined Cell
398 Migration. *Annu Rev Biomed Eng.* 2016;159–80. 1
- 399 4. Wells A, Grahovac J, Wheeler S, Ma B, Lauffenburger D. Targeting tumor cell motility as a
400 strategy against invasion and metastasis. *Trends Pharmacol Sci.* 2013;283–9
- 401 5. Odenwald MA, Prosperi JR, Goss KH. APC/β-catenin-rich complexes at membrane protrusions
402 regulate mammary tumor cell migration and mesenchymal morphology. *BMC Cancer*
403 2013;12.
- 404 6. Cowden Dahl KD, Dahl R, Kruichak JN, Hudson LG. The epidermal growth factor receptor
405 responsive miR-125a represses mesenchymal morphology in ovarian cancer cells.
406 *Neoplasia* 2009;1208–15.
- 407 7. Prasad A, Alizadeh E. Cell Form and Function: Interpreting and Controlling the Shape of
408 Adherent Cells. *Trends Biotechnol.* 2018
- 409 8. Wu P-H, Gilkes DM, Phillip JM, Narkar A, Cheng TW-T, Marchand J, et al. Single-cell
410 morphology encodes metastatic potential. *Sci Adv.* 2020
- 411 9. Lyons SM, Alizadeh E, Mannheimer J, Schuamberg K, Castle J, Schroder B, et al. Changes in
412 cell shape are correlated with metastatic potential in murine and human osteosarcomas.
413 *Biol Open.* 2016;289 – 299
- 414 10. Alizadeh E, Lyons SM, Castle JM, Prasad A. Measuring systematic changes in invasive
415 cancer cell shape using Zernike moments. *Integr Biol.* 2016;1183–93.
- 416 11. Valastyan S, Weinberg RA. Tumor metastasis: molecular insights and evolving paradigms.
417 *Cell.* 2011;275–92.
- 418 12. Shieh AC. Biomechanical Forces Shape the Tumor Microenvironment. *Ann Biomed Eng.*
419 2011;1379–89.

- 420 13. Provenzano PP, Inman DR, Eliceiri KW, Knittel JG, Yan L, Rueden CT, et al. Collagen density
421 promotes mammary tumor initiation and progression. *BMC Med.* 2008.
- 422 14. Wershof E, Park D, Jenkins RP, Barry DJ, Sahai E, Bates PA. Matrix feedback enables
423 diverse higher-order patterning of the extracellular matrix. *PLOS Comput Biol.* 2019.
- 424 15. Kawecki TJ, Lenski RE, Ebert D, Hollis B, Olivieri I, Whitlock MC. Experimental evolution.
425 *Trends Ecol Evol.* 2012;547–60
- 426 16. Sprouffske K, Merlo LMF, Gerrish PJ, Maley CC, Sniegowski PD. Cancer in light of
427 experimental evolution. Vol. 22, *Current Biology*. 2012.
- 428 17. Taylor TB, Johnson LJ, Jackson RW, Brockhurst MA, Dash PR. First steps in experimental
429 cancer evolution. *Evol Appl.* 2013;535–48.
- 430 18. Taylor TB, Wass A V, Johnson LJ, Dash P. Resource competition promotes tumour
431 expansion in experimentally evolved cancer. *BMC Evol Biol.* 2017;268.
- 432 19. Chaffer CL, Weinberg RA. A Perspective on Cancer Cell Metastasis. *Science.* 2011;1559 –
433 1564.
- 434 20. Pantel K, Brakenhoff RH. Dissecting the metastatic cascade. *Nat Rev Cancer.* 2004;448–56.
- 435 21. Massagué J, Obenauf AC. Metastatic colonization by circulating tumour cells. *Nature.*
436 2016;298–306. 0
- 437 22. Clark AG, Vignjevic DM. Modes of cancer cell invasion and the role of the microenvironment.
438 *Curr Opin Cell Biol.* 2015;13–22.
- 439 23. Peinado H, Lavotshkin S, Lyden D. The secreted factors responsible for pre-metastatic niche
440 formation: Old sayings and new thoughts. *Semin Cancer Biol.* 2011;139–46.
- 441 24. Scneay J, Smyth MJ, Möller A. The pre-metastatic niche: finding common ground. *Cancer*
442 *Metastasis Rev.* 2013;449–64.
- 443 25. Psaila B, Kaplan RN, Port ER, Lyden D. Priming the “soil” for breast cancer metastasis: the
444 pre-metastatic niche. *Breast Dis.* 2015;26:65–74.
- 445 26. Costa-Silva B, Aiello NM, Ocean AJ, Singh S, Zhang H, Thakur BK, et al. Pancreatic cancer
446 exosomes initiate pre-metastatic niche formation in the liver. *Nat Cell Biol.* 2015;816–26.
- 447 27. Keeton SJ, Delalande JM, Cranfield M, Burns A, Dash PR. Compressed collagen and
448 decellularized tissue – novel components in a pipeline approach for the study of cancer
449 metastasis. *BMC Cancer.* 2018;622.
- 450 28. Medberry CJ, Crapo PM, Siu BF, Carruthers CA, Wolf MT, Nagarkar SP, et al. Hydrogels
451 derived from central nervous system extracellular matrix. *Biomaterials.* 2013;1033–40.
- 452 29. Quatromoni JG, Singhal S, Bhojnagarwala P, Hancock WW, Albelda SM, Eruslanov E. An
453 optimized disaggregation method for human lung tumors that preserves the phenotype
454 and function of the immune cells. *J Leukoc Biol.* 2015;201–9.
- 455 30. Tsai HF, Gajda J, Sloan TFW, Rares A, Shen AQ. Usiigaci: Instance-aware cell tracking in
456 stain-free phase contrast microscopy enabled by machine learning. *SoftwareX.* 2019;230–
457 7.
- 458 31. Schindelin J, Arganda-Carreras I, Frise E, Kaynig V, Longair M, Pietzsch T, et al. Fiji: an
459 open-source platform for biological-image analysis. *Nat Methods.* 2012;676–82.
- 460 32. Van Rossum G, Drake FL. Python 3 Reference Manual. Scotts Valley, CA: CreateSpace;
461 2009.
- 462 33. Zernike F. Phase contrast, a new method for the microscopic observation of transparent
463 objects part II. *Physica.* 1942;974–86.
- 464 34. Liao SX. Image Analysis by Moments. The University of Manitoba; 1994.
- 465 35. R Core Team. R: A Language and Environment for Statistical Computing. 2017
- 466 36. Wickham H. ggplot2: Elegant Graphics for Data Analysis. Springer-Verlag New York2009.
- 467 37. Bolker BM, Brooks ME, Clark CJ, Geange SW, Poulsen JR, Stevens MHH, et al. Generalized
468 linear mixed models: a practical guide for ecology and evolution. *Trends Ecol Evol.*
469 2009;127–35.
- 470 38. Nakagawa S, Schielzeth H. A general and simple method for obtaining R2 from generalized
471 linear mixed-effects models. *Methods Ecol Evol.* 2013;133–42.
- 472 39. Liu H-S, Jan M-S, Chou C-K, Chen P-H, Ke N-J. Is Green Fluorescent Protein Toxic to the
473 Living Cells? *Biochem Biophys Res Commun.* 1999;712–7.

- 474
475 40. Bollen KA, Jackman RW. Regression Diagnostics: An Expository Treatment of Outliers and
476 Influential Cases. *Sociol Methods Res.* 1985;510–42.
477 41. Staneva R, El Marjou F, Barbazan J, Krndija D, Richon S, Clark AG, et al. Cancer cells in the
478 tumor core exhibit spatially coordinated migration patterns. *J Cell Sci.* 2019. t
479 42. Yuan Y. Spatial Heterogeneity in the Tumor Microenvironment. *Cold Spring Harb Perspect
Med.* 2016.
480 43. Anguiano M, Castilla C, Maška M, Ederra C, Peláez R, Morales X, et al. Characterization of
481 three-dimensional cancer cell migration in mixed collagen-Matrigel scaffolds using
482 microfluidics and image analysis. *PLoS One.* 2017;7.
483 44. Pavel M, Renna M, Park SJ, Menzies FM, Ricketts T, Füllgrabe J, et al. Contact inhibition
484 controls cell survival and proliferation via YAP/TAZ-autophagy axis. *Nat Commun.*
485 2018;2961
486 45. Petrie RJ, Yamada KM. At the leading edge of three-dimensional cell migration. *J Cell Sci.*
487 2012;5917–26.
488 46. Malanchi I, Santamaria-Martínez A, Susanto E, Peng H, Lehr H-A, Delaloye J-F, et al.
489 Interactions between cancer stem cells and their niche govern metastatic colonization.
490 *Nature.* 2012;85–9.
491 47. Page-McCaw A, Ewald AJ, Werb Z. Matrix metalloproteinases and the regulation of tissue
492 remodelling. Vol. 8, *Nature Reviews Molecular Cell Biology.* 2007.
493
494

495 **Figures**
496



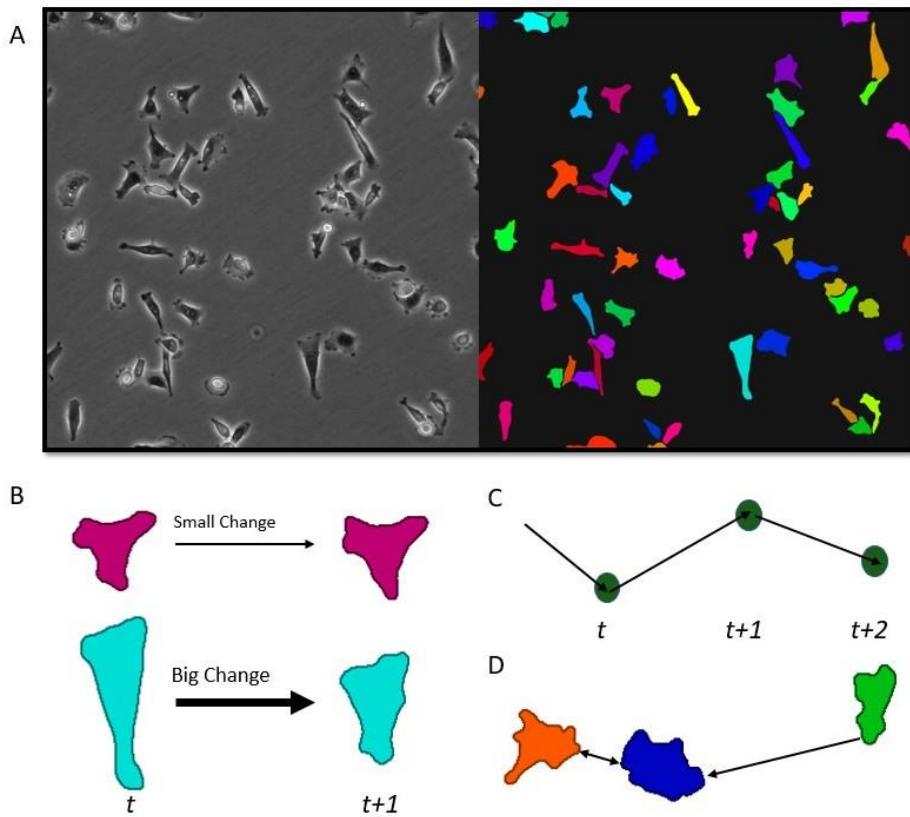
497
498 **Figure 1. Experimental evolution of cancer cell populations.** Ancestor populations were kept
499 frozen throughout. Escape populations were placed in a high density collagen matrix the
500 surrounded by a low density outer collagen ring: after 10-14 days cells that had escaped into the
501 outer ring (shown in blue) were released, expanded and reseeded back into a new high density
502 collagen core; this process was repeated 7 times over the course of 6 months. Invasion
503 populations were seeded around a Matrigel island; after 7 days cells that had invaded the
504 Matrigel (shown in blue) were released, expanded and reseeded around a new Matrigel island
505 this was repeated 15 times over the course of 6 months. Colonisation populations were seeded
506

507 onto a piece of decellularized rat lung which acted as a novel scaffold for colonisation and left to
508 establish for 6 months. Four replicate lines were maintained for each treatment.

509

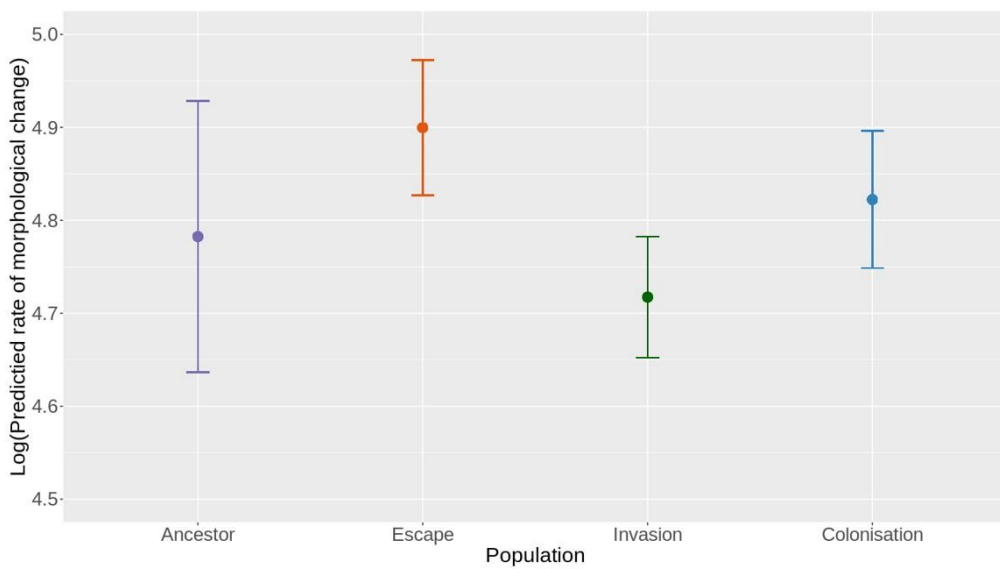
510

511



512
513
514
515
516
517
518
519
520
521
522
523
524

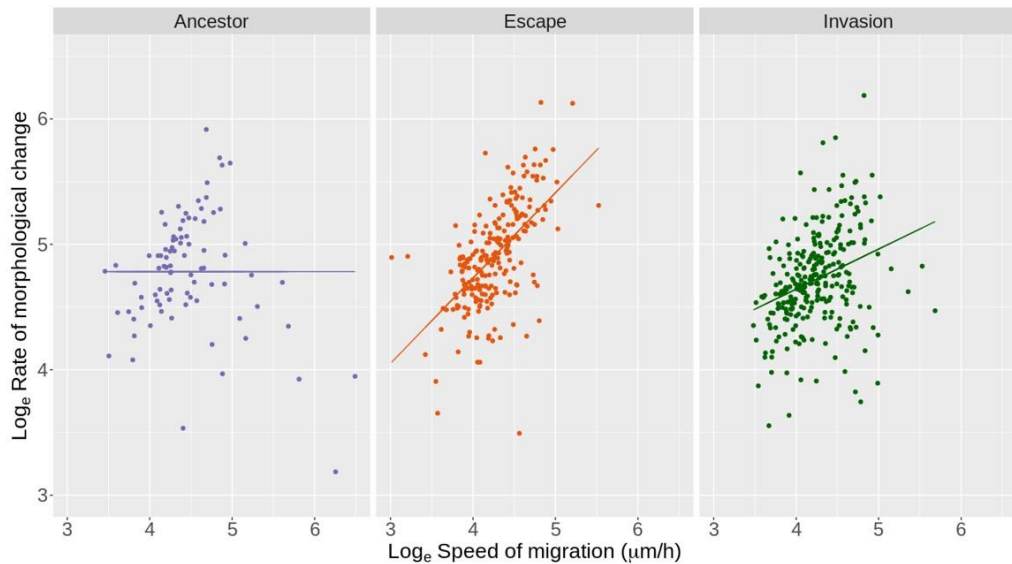
Figure 2. Quantifying dispersal from time-lapse videos. (A) Cells were tracked over a 12 hour period with images taken at two minute intervals using phase contrast time-lapse microscopy to generate movies from which morphology could be segmented through the use of a convolutional neural network. (B) The rate of morphological change was recorded as the distance between Zernike moments in consecutive frames. (C) The speed of migration is calculated as the distance between the spatial location of cells in consecutive frames. (D) The distance between neighbouring cells is quantified as the shortest distance between the contour of one cell and the contour of another. The direction of the arrow points from a given cell to the point on the contour of the closest neighbouring cell.



525

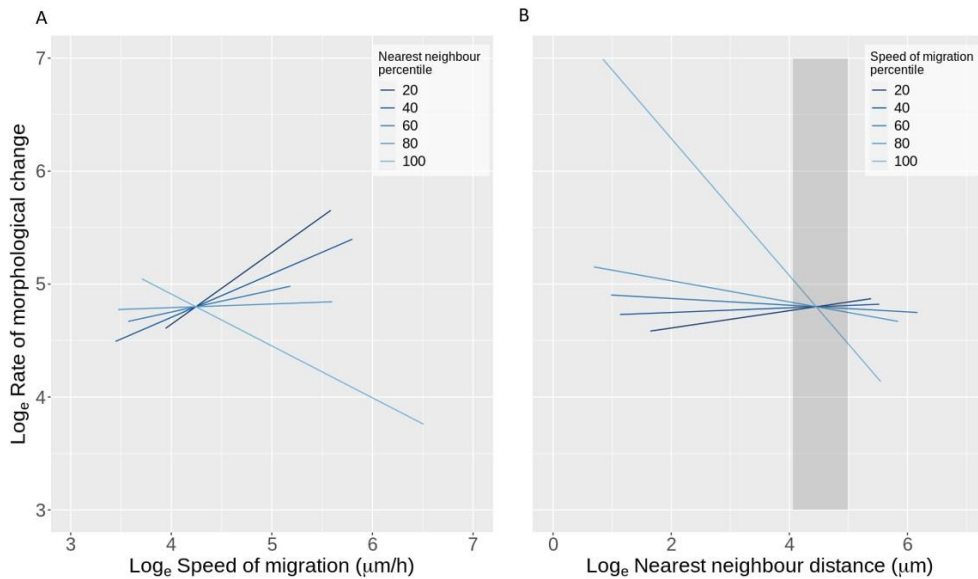
526 **Figure 3. Comparing the mean rate of morphological change among the four treatments.** A
 527 plot of the natural log-transformed rate of morphological change for each of the four treatments.
 528 The centre dot signifies the mean rate of morphological change with errors bars signifying 95%
 529 confidence intervals. The escape populations had a significantly faster rate of morphological
 530 change compared with the invasion populations, $p = 0.0152$ ($N = 813$). The mean, standard error
 531 and number of observations for each population can be found in Table S1.

532



533

534
 535 **Figure 4. The rate of morphological change against the speed of migration.** The natural log-
 536 transformed rate of morphological change plotted against the natural log-transformed speed of
 537 migration. The straight lines represent the reduced model for each treatment using only
 538 parameters that are significant at the 5% level. The ancestor populations have an intercept-only
 539 model fitted ($N = 88$). The speed of migration is the only significant variable in the escape ($N =$
 540 230 , $p = 1.765 \times 10^{-3}$) and invasion ($N = 283$, $p = 0.018$) populations. For both escape and
 541 invasion populations the rate of morphological change is positively correlated with the speed of
 migration, the faster the speed of migration the higher the rate of morphological change.



542
 543 **Figure 5. A dynamic switch in the morphological behaviour within cells selected for**
 544 **colonisation.** Data points have been removed to highlight the behaviour of the model, the same
 545 model with data points can be seen in Fig. S2. The speed of migration ($p = 5.418 \times 10^{-14}$), the
 546 distance to the nearest neighbouring cell ($p = 2.207 \times 10^{-10}$) and the interaction of the two ($p =$
 547 2.219×10^{-11}) was significant in the colonisation population ($N = 212$). (A) The predicted natural
 548 log-transformed rate of morphological change against the natural log-transformed speed of
 549 migration. The shaded lines indicate the natural log transformed nearest neighbour percentile.
 550 The lighter the line, the further away from a neighbouring cell with distance values ranging
 551 from $2\mu\text{m}$ - $477\mu\text{m}$. (B) The predicted natural log-transformed rate of morphological change against the
 552 natural log-transformed nearest neighbour distance. The shaded lines indicate the speed of
 553 migration percentile. The lighter the line the faster the speed of migration. The shaded region
 554 indicates the range of distances over which there is no significant relationship in the rate of
 555 morphological change and the speed of migration when the data is centred at these distances,
 556 between $57.9\mu\text{m}$ and $147.2\mu\text{m}$.

557
 558
 559
 560
 561